

**Kinetics of T-cell receptor-dependent  
antigen recognition determined *in vivo*  
by multi-spectral normalized  
epifluorescence laser scanning**

Rosy Favicchio  
Giannis Zacharakis  
Katerina Oikonomaki  
Athanasios Zacharopoulos  
Clio Mamalaki  
Jorge Ripoll

# Kinetics of T-cell receptor-dependent antigen recognition determined *in vivo* by multi-spectral normalized epifluorescence laser scanning

Rosy Favicchio,<sup>a,b</sup> Giannis Zacharakis,<sup>b</sup> Katerina Oikonomaki,<sup>a</sup> Athanasios Zacharopoulos,<sup>b</sup> Clio Mamalaki,<sup>a</sup> and Jorge Ripoll<sup>b</sup>

<sup>a</sup>Institute of Molecular Biology and Biotechnology, Foundation for Research and Technology-Hellas, 71110 Heraklion, Crete, Greece

<sup>b</sup>Institute of Electronic Structure and Laser, Foundation for Research and Technology-Hellas, 71110 Heraklion, Crete, Greece

**Abstract.** Detection of multiple fluorophores in conditions of low signal represents a limiting factor for the application of *in vivo* optical imaging techniques in immunology where fluorescent labels report for different functional characteristics. A noninvasive *in vivo* Multi-Spectral Normalized Epifluorescence Laser scanning (M-SNELS) method was developed for the simultaneous and quantitative detection of multiple fluorophores in low signal to noise ratios and used to follow T-cell activation and clonal expansion. Colocalized DsRed- and GFP-labeled T cells were followed in tandem during the mounting of an immune response. Spectral unmixing was used to distinguish the overlapping fluorescent emissions representative of the two distinct cell populations and longitudinal data reported the discrete pattern of antigen-driven proliferation. Retrieved values were validated both *in vitro* and *in vivo* with flow cytometry and significant correlation between all methodologies was achieved. Noninvasive M-SNELS successfully quantified two colocalized fluorescent populations and provides a valid alternative imaging approach to traditional invasive methods for detecting T cell dynamics. © 2012 Society of Photo-Optical Instrumentation Engineers (SPIE). [DOI: 10.1117/JBO.17.7.076013]

Keywords: multispectral imaging; fluorescence; imaging systems; epifluorescence imaging; population dynamics; laser scanning.

Paper 11768 received Dec. 19, 2011; revised manuscript received May 7, 2012; accepted for publication May 23, 2012; published online Jul. 9, 2012.

## 1 Introduction

The retrieval of quantitatively accurate and proportionally comparable concentration values for two or more fluorescent proteins represents a significant challenge for current *in vivo* optical imaging systems. The main difficulty in simultaneous detection of fluorescence intensities from more than one spectral region is represented by the variability in light attenuation associated with the wavelength-dependent tissue optical properties. The implication is that emission intensities of two different fluorescent proteins measured with separate filters cannot be directly compared to each other, in particular when the emissions overlap. Rather, an analytical approach is required, as is already in place for 3-dimensional imaging modalities.<sup>1</sup> In fluorescence molecular tomography (FMT),<sup>2-4</sup> the normalization of the emission with the excitation intensities is a well-established method of accounting for tissue optical heterogeneities and represents the basis to obtain quantitative feedback.<sup>5,6</sup> More recently, optical imaging methodologies have enabled the quantitative detection of combined fluorescent signals based on multispectral data collection and linear unmixing algorithms.<sup>7-11</sup> Yet, the major limitation when using 3-dimensional optical tomography within the visible range is the signal to noise ratio (SNR), affected greatly by blood absorption and tissue autofluorescence levels (particularly high between 500 and 600 nm). Low SNR levels affect depth resolution and restrict fluorescence detection to superficial objects that can

nevertheless be detected using 2-dimensional planar methodologies.<sup>12-14</sup> We reasoned that, combining multi spectral unmixing algorithms with the use of normalized epifluorescence intensities would result in the simultaneous and quantitative detection of multiple fluorescent proteins from superficial objects, even in low SNR regimes.

The feasibility of Multi-Spectral Normalized Epifluorescence Laser scanning (M-SNELS) as a noninvasive optical imaging modality was addressed at monitoring T cell population dynamics *in vivo*. T-cells function as active sentinels through the circulatory and lymphatic systems. The mechanisms driving stages of T-cell activation, differentiation, migration, and clonal expansion depend on crosstalk between different cell populations and represent an ideal *in vivo* imaging model. In particular, T-cell proliferation is a fundamental parameter for a vigorous and successful immune response against pathogens and is also a diagnostic/prognostic marker in autoimmune diseases. Adoptive T cell transfer is commonly used to monitor transgenic T-cell receptor (TCR)-specific responses in lymphopenic hosts. The traditional methodologies used to detect T-cell proliferation require the harvesting of fluorescently labeled cells from primary and secondary lymphoid organs, followed by fluorescence activated cell sorting (FACS) analysis. Alternatively, radiolabeling of newly synthesized DNA can be used to quantify proliferation, as well as antibody-based staining techniques (e.g., BrdU and Ki-67). Although cell sorting and radio labeling provide quantitative information and accurate values on individual samples, understanding the kinetics of T cell proliferation is nevertheless hindered by inter-subject heterogeneity. A recent

Address all correspondence to: Rosy Favicchio, Institute of Molecular Biology and Biotechnology, Foundation for Research and Technology-Hellas, 71110 Heraklion, Crete, Greece. Tel: +(30) 2810391912; E-mail: [rosy@imbb.forth.gr](mailto:rosy@imbb.forth.gr)

study highlighted that variation in gene expression *in vivo* is predominant in genes modulated by the immune system.<sup>15</sup> This suggests that “natural variability” in a T cell population should be taken into account for analyzing elements of the immune response, especially when using lymphopenic hosts.<sup>16</sup> Several reports have illustrated T cell dynamics *in vivo* using bioluminescence, alone<sup>17–19</sup> or in combination with positron emission tomography,<sup>20,21</sup> where the bioluminescent signal was restricted to a single T-cell population. *Ex vivo*, two distinct fluorescent probes were detected using a spectral differentiation module fitted to a cryotome.<sup>22</sup> Two-photon fluorescence microscopy was instead successful in imaging two distinct fluorescent populations highlighting cell interactions, cell-to-cell contacts and migration.<sup>23,24</sup> The dynamics determined by intravital microscopy span timeframes in the range of minutes/hours and are ideally suited for describing rapid movements with single cell resolution (e.g., contact time and velocity). However, no method has been established in small animal models for the simultaneous and quantitative detection of multiple and colocalized populations *in vivo* with timeframes in the order of hours/days/months. Quantitative population dynamics could be used to monitor migration and proliferation and elucidate the differences between antigen-driven expansion and homeostatic control mechanisms.

Here, to illustrate the strength in applying M-SNELS to immunological research, multicolor unmixing was used to follow the *in vivo* dynamics of antigen recognition by simultaneous detection of a responding and a nonresponding T cell population. The F5/DsRed-expressing<sup>25</sup> T cells used in this experiment expressed the TCR that recognized a nine amino acid sequence of the influenza virus nucleoprotein (NP).<sup>26</sup> The administration of the NP synthetic peptide affects the response of these lymphocytes, restricted by class I major histocompatibility complex, and leads to a rapid increase of their population.<sup>27,28</sup> The CD2/GFP-expressing T-cells on the other hand,<sup>29</sup> do not express the specific TCR and do not respond to NP stimulation. Experiments were performed using the Rag1-deficient mouse (Rag1<sup>-/-</sup>) that lacks functional RAG1 (recombination-activating gene -1) protein.<sup>30–32</sup> These mice do not develop T-cells or B-cells and are, thus, immunodeficient. T cell responses of both responsive and nonresponsive populations were followed over a 5-day period after intraperitoneal injection of the antigen-presenting NP peptide. M-SNELS quantification was independently assessed *in vitro* and using FACS, demonstrating that M-SNELS reports on the temporal dynamics of T-cell proliferation *in vivo*.

## 2 Materials and Methods

### 2.1 Multi-Spectral Normalized Epifluorescence Laser Scanning Setup

A schematic representation of the M-SNELS setup is shown in Fig. 1. Illumination is provided by a cw Argon-Ion Laser (Laser Physics, Reliant 1000 m, West Jordan, UT 84088), emitting at 458, 488, and at 514.5 nm. The laser light is directed to the imaging chamber through a series of mirrors (Edmund Optics) and into an optical scanner (Scancube 7, Scanlab, Germany); its miniaturized galvanometer motors were controlled by in-house developed software and the laser beam was scanned on the *x-y* plane of the sample. The setup was dedicated to superficial objects and images were recorded in reflection geometry mode. The sample holder consisted of a plate of black,

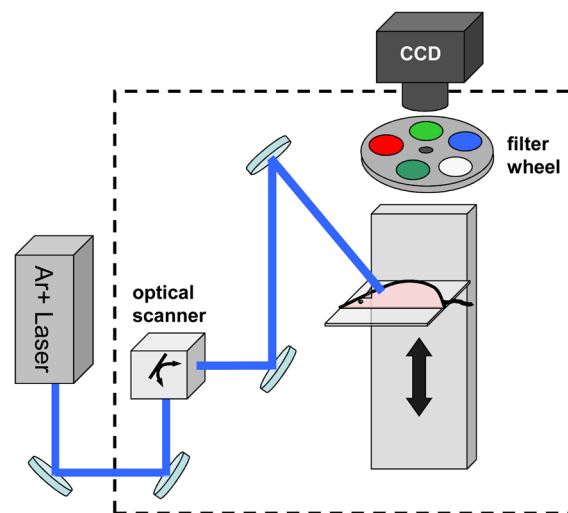


**Fig. 1** Multi-spectral Normalized Epifluorescence Laser scanning setup. A diagrammatic representation of the setup developed for Multi-Spectral Normalized Epifluorescence Laser Scanning is shown. An Argon ion laser is directed through a series of mirrors into the imaging chamber and into an optical scanner that in turn scans the region of interest of the mouse. An image is recorded for each laser position by a CCD camera linked to a PC. This process is repeated for all filter combinations.

anti-reflecting material mounted on *x-y-z* translation stages. Images were acquired by a thermoelectrically cooled 16-bit CCD camera (Andor Corp., DV434, Belfast, Northern Ireland), mounted on the top of the imaging chamber. The CCD camera was equipped with a SIGMA 50-mm *f*/2.8 objective (Sigma Corporation, Tokyo, Japan), focused on the sample’s surface. A filter wheel mounted in front of the CCD camera lens with different bandpass interference filters enabled the acquisition of multi-spectral data. Excitation measurements were recorded using the 488 nm  $\pm$ 30 nm and 510 nm  $\pm$ 5 nm filters and the fluorescence measurements were recorded using 540 nm  $\pm$ 20 nm and 615 nm  $\pm$ 45 nm filters (Andover Corporation).

### 2.2 *In vivo* Image Acquisition

Anesthetized animals ( $n = 13$ ) were placed on the sample holder and the experimental parameters were defined. Exposure time, excitation power, number, and pattern of the illumination points (sources) were set according to the size and shape of the sample and the resolution requirements of each specific experiment. The adaptability of the pattern and number of sources was a benefit of the optical scanner and provided a great advantage when dealing with live samples, where size and shape of the target may vary significantly. The parameters were optimized on nine control animals (sacrificed after each imaging session for *ex vivo* validation), and applied to the peptide response experiment (four animals, repeatedly imaged *in vivo*). The optimized parameters consisted of a  $12 \times 7$  source scan pattern covering a field of view of  $10 \times 7$  mm<sup>2</sup>, exposure times of 0.1 to 0.2 s for the excitation light and 0.6 to 0.8 s for fluorescence light, for DsRed and GFP, respectively. The experimental measurements consisted of a series of scanned acquisitions, first for the fluorescence light (excitation/emission: 488 nm/540 nm; 488 nm/615 nm; 514 nm/540 nm; 514 nm/615 nm) and then for the excitation light (at 488 nm  $\pm$ 30 nm and 510 nm  $\pm$ 5 nm), each mouse was therefore scanned six times in order to perform multi-spectral unmixing. Summing these

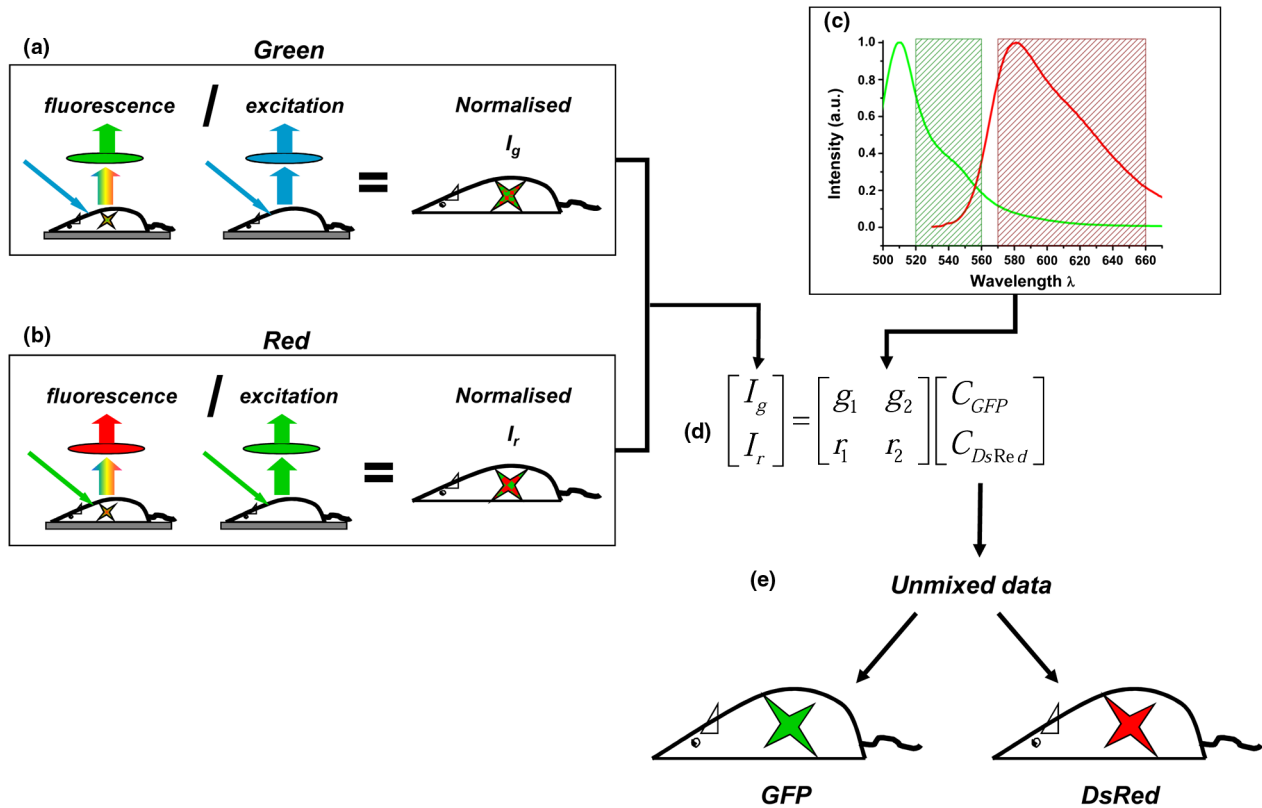


**Fig. 2** M-SNELS imaging protocol. The acquisition method used for Multi-spectral Normalized Epifluorescence Laser scanning is shown for the filter combinations used: (a) the green channel uses a 488-nm excitation and a 540/40-nm filter, whereas the red channel (b) uses a 514-nm excitation source and a 635/90-nm emission filter. A fluorescence and excitation measurement is recorded for each channel by switching the filters. (c) GFP and DsRed emission profiles are shown together with the emission filter bands used for M-SNELS image acquisitions, indicating the proportion of overlap displayed by these two fluorophores. (d) The normalized measurements and spectral strengths are fed into the Multi Spectral unmixing algorithm and (e) the resulting unmixed data represent the “clean” GFP and DsRed concentration values.

acquisitions, as shown in Eqs. (1) and (2), results in the fluorescence and excitation images.

$$U_{fl} = \sum_{i=1}^k (I_{fl}^k - B_{fl}) \quad (1)$$

$$U_{exc} = \sum_{i=1}^k (I_{exc}^k - B_{exc}), \quad (2)$$

where  $U_{fl}$  and  $U_{exc}$  are the fluorescence and excitation images,  $I_{fl}^k$  and  $I_{exc}^k$  are the fluorescence and excitation measurements, respectively, for the  $k$ 'th source.  $B_{fl}$  and  $B_{exc}$  are the background measurements for fluorescence and excitation, respectively, obtained with the same settings but without the excitation light. Each excitation measurement was used here to normalize its corresponding fluorescence measurement on a source-to-source basis. This step effectively accounts for the heterogeneities encountered by light propagation through tissue. Hence, the final images used for the calculations were obtained after dividing (normalizing) the fluorescence with the excitation as shown in Eq. (3):

$$U_{norm} = \frac{U_{fl}}{U_{exc}} = \frac{\sum_{i=1}^k (I_{fl}^k - B_{fl})}{\sum_{i=1}^k (I_{exc}^k - B_{exc})}. \quad (3)$$

Such an approach is necessary for obtaining quantitative results as demonstrated for FMT.<sup>5,6</sup> If more than one fluorescent target needs to be imaged, as in this case for GFP and DsRed, the above

measurements need to be performed in two detection channels corresponding to the two bandpass emission filters described earlier. In order to separate the individual signals of the two fluorophores, a spectral unmixing algorithm was used.

### 2.3 Spectral Unmixing

Spectral unmixing methods exploit the fact that the detected fluorescence signal can be expressed as a linear combination of the different fluorescent components present in the sample. A linear equation can thus be derived for each detection channel, corresponding to the sum of the concentration of the fluorescence emitters multiplied by a weighting factor equivalent to the strength of the emission for each specific channel. Hence, in the case where the number of detection channels is equal to the number of investigated fluorescence targets a well-defined system of equations can be derived and solved to calculate the unknown concentrations, as shown in Eq. (4):

$$I_g = g_1 C_{GFP} + g_2 C_{DsRed} \quad I_r = r_1 C_{GFP} + r_2 C_{DsRed}, \quad (4)$$

where  $I_g$ ,  $I_r$  are the fluorescence images obtained for the detection channels of GFP and DsRed,  $g_1$ ,  $g_2$ ,  $r_1$  and  $r_2$  are the spectral strengths of GFP and DsRed, respectively, while the subindex represents the two filters used for measurement.  $C_{GFP}$  and  $C_{DsRed}$  are the unknown concentrations of each fluorophore. If the previous system is expressed in matrix notation we obtain:

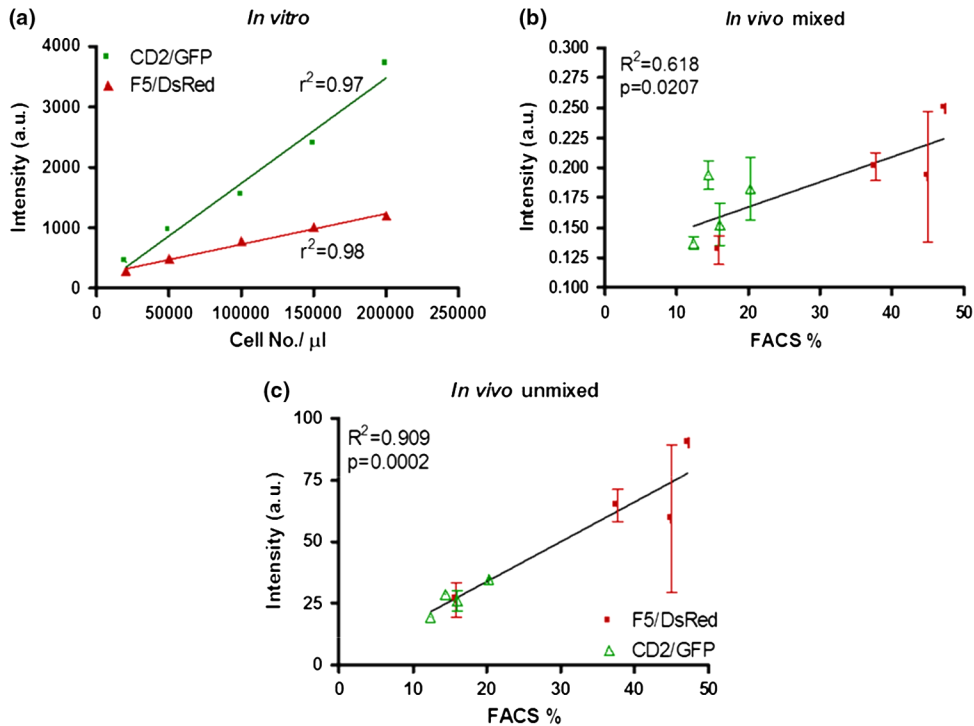


**Fig. 3** M-SNELS unmixing retrieves quantitative information *in vitro* and *in vivo*. (a) *In vitro* calibration was performed using increasing concentrations of GFP and DsRed cells in culture. Five cell concentrations (20,000 to 200,000 cells/ $\mu$ l) were plated in a fixed total volume of 10  $\mu$ l and imaged using M-SNELS. The normalized fluorescence intensities for each sample were fitted to a linear regression model and show excellent correlation to the cell concentrations. (b) to (c) M-SNELS was applied *in vivo* to measure the change in CD2/GFP and F5/DsRed T-cell populations following peptide treatment in the cervical LNs. Rag1<sup>-/-</sup> mice ( $n = 4$ ) received equal numbers of CD2/GFP and F5/DsRed cells by adoptive transfer and underwent NP peptide treatment 12 days later. Validation of M-SNELS unmixing *in vivo* was carried out by comparing the M-SNELS intensity values to the percentage (%) of fluorescent cells recovered by FACS on the same day. Left and right cervical LNs were individually quantified (for each fluorophore) with both methodologies, the averaged left and right node values, were plotted. Linear regression analysis (b) before ( $r^2 = 0.618$ ;  $p = 0.0207$ ) and (c) after ( $r^2 = 0.909$ ;  $p = 0.0002$ ) unmixing illustrates the value of M-SNELS as it enables the quantitative comparison of multiple reporters within the same animal. Data correspond to mean  $\pm$  SD.

$$\begin{bmatrix} I_g \\ I_r \end{bmatrix} = \begin{bmatrix} g_1 & g_2 \\ r_1 & r_2 \end{bmatrix} \begin{bmatrix} C_{GFP} \\ C_{DsRed} \end{bmatrix}. \quad (5)$$

$$\begin{bmatrix} C_{GFP} \\ C_{DsRed} \end{bmatrix} = \begin{bmatrix} g_1 & g_2 \\ r_1 & r_2 \end{bmatrix}^{-1} \begin{bmatrix} I_g \\ I_r \end{bmatrix}. \quad (6)$$

The solution of the above system is given by the following equation that provides the unknown concentrations:

The values of the spectral strengths were calculated by measuring, separately, each cell population (carrying either GFP or DsRed as a reporter) with the M-SNELS setup. Emission intensities were recorded by exciting the fluorophores at the two

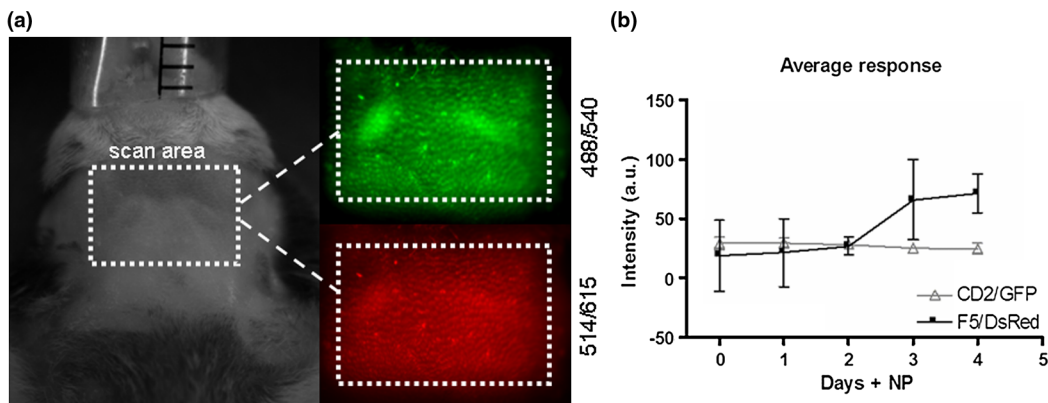


**Fig. 4** M-SNELS imaging the dynamics of an antigen-dependent response. (a) Left and right cervical LNs are shown for a mouse as recorded by M-SNELS in the green (ex488 nm-em540/40 nm) and red channels (ex514 nm-em615/90 nm) in low SNR regimes (ranging from 1:1 to 4:1). (b) The dynamic behavior of the antigen-dependent response was observed by following the increase over time in sensitized F5/DsRed cells. Within the same time frame, the nonresponsive CD2/GFP cells did not proliferate. Data correspond to mean  $\pm$  SD.

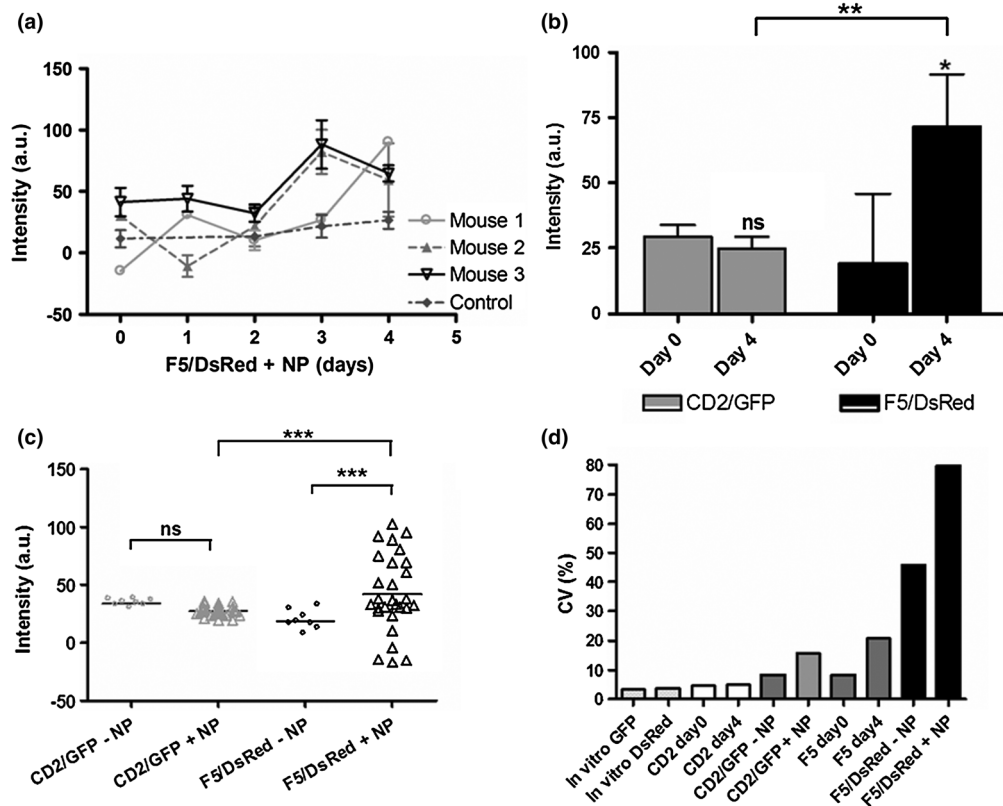


**Fig. 5** M-SNELS quantification of CD2/GFP and F5/DsRed responses to peptide. M-SNELS imaging was used to follow the *in vivo* kinetics of two colocalized populations. NP responsive (F5/DsRed) and nonresponsive (CD2/GFP) T cell populations were detected simultaneously over a 5-day time course, following the injection of NP peptide. (a) The time-frame of the response to peptide stimulation for individual F5/DsRed populations illustrates how similar magnitude in overall response can be achieved by variable temporal dynamics. (b) T cell-specific response to peptide was assessed using a paired *t* test between data recorded on days 0 (before treatment) and 4 (after treatment) for the two populations. Only the treated F5/DsRed show significant increase between the two time points, confirming a specific response to the treatment. (c) Scatter plot of unmixed CD2/GFP and F5/DsRed fluorescence data during a 5-day timeframe show a significant increase in distribution of values in the F5/DsRed population treated with peptide (+NP), compared to the CD2/GFP population (in the same animals) and to untreated samples (*F* test). (d) The accuracy of M-SNELS in describing animal heterogeneity was assessed by comparing the coefficient of variation (CV) of longitudinal data (-NP and +NP) against the CV on individual days (day 0 and day 4) and against the CV of *in vitro* data describing the precision and reproducibility of M-SNELS results and that were considered, in this scenario, representative of M-SNELS systematic error. The sharp increase in variation displayed by F5/DsRed data, particularly after peptide treatment and not on day 0, indicates that M-SNELS is sensitive to T-cell dependent animal heterogeneity. Data correspond to mean  $\pm$  SD.

wavelengths used (488 and 514 nm). Since the intensity of each emission depends on its concentration, the spectral strengths were calculated by the difference in emission intensities corresponding to the spectral band allowed by each filter used during image acquisition. The numerical results of these calculations are reported in Table 1. The M-SNELS spectral unmixing method was developed by building on previously characterized spectral properties of skin autofluorescence and attenuation of fluorescent signal,<sup>7</sup> resulting in the negative  $g_{DsRed}$  value. These negative values effectively result in a proportion of signal (i.e., autofluorescence) being removed; however, no additional autofluorescence measurement is performed during the experiment. Following M-SNELS unmixing, data that correspond to autofluorescence become negative. In our method therefore, any positive value corresponds to specific fluorescence where values below the baseline (zero) correspond to autofluorescence.

## 2.4 Mice

Protocols involving the use of animals were conducted in accordance with and under the approval of the Foundation for

Research and Technology Ethics Committee. All mouse lines (Rag1<sup>-/-</sup>, F5/DsRed, and CD2/GFP) were housed and bred in the animal facilities of the Institute of Molecular Biology and Biotechnology (IMBB-FORTH) following national and institutional guidelines for animal handling. For the protocols described here, mice were anesthetized with 1.5% to 2.5% isoflurane (Isoflurane Vaporiser, LumicInternational), delivered initially in a tranquilizing chamber and subsequently using a mask during the imaging sessions.

## 2.5 Adoptive Transfer of Splenocytes in Lymphopenic Recipients

Splenocytes were isolated from a total of 15 F5/DsRed and CD2/GFP-expressing transgenic mice. GFP and DsRed positive cells were counted using FACS and  $5 \times 10^4$  cells each of GFP and DsRed T-cells were pooled together and transferred through tail vein injection in Rag1<sup>-/-</sup> immunodeficient mice twelve days prior to the first imaging session and NP peptide injection (day 0).

## 2.6 Peptide Administration in Lymphopenic Recipients

Fifty nmol of synthetic peptide sequence from the influenza virus nucleoprotein [NP-(366-374)]<sup>27</sup> was administered intraperitoneally with phosphate buffered saline (1xPBS) in three animals and the control animal was treated with an equal volume of 1xPBS. Great care was devoted in assuring all animals received identical treatment throughout the experimental time frame. For this purpose siblings were chosen and underwent all procedures (adoptive transfer, peptide administration, imaging sessions, and flow cytometric analysis) simultaneously. The use of four animals was instrumental and limited by the number of animals that could, in practice, be treated identically.

## 2.7 Flow Cytometric Analysis

Single cell suspensions were obtained from the spleen (for the adoptive transfer) and the cervical LNs for control animals and on day 4 for the antigen-response experiment and analyzed using FACS. Splenocytes were purified from red blood cells via a water lysis step.

Cervical LNs vary in terms of size, number and anatomical location between animals. Therefore, in order to match the number of lobes imaged with M-SNELS each animal was dissected under a fluorescent stereomicroscope. The superficial and clearly visible lobes were gathered and treated as left and right nodes (one or two lobes per side). For dual fluorophore detection by flow cytometry, approximately 10,000 events were collected for each sample using the FL1 and FL2 detectors of a FACS Calibur (BD Biosciences, San Jose, CA) by setting 1.8%-FL1 and 17.9%-FL2 compensation and analyzed using CellQuest software (BD Biosciences, San Jose, CA).

## 2.8 In Vitro M-SNELS Imaging of Cell Culture

Splenocytes were extracted from one F5/DsRed and one CD2/GFP mouse, isolated from red blood cells via water lysis and counted using FACS. Splenocytes were resuspended in PBS at five different concentrations (20,000 to 200,000 cells/ $\mu$ l) and plated in a 96-well cell culture plate in a total volume of 10  $\mu$ l (cell numbers and total volume were chosen to match those of a typical LN). The plate was placed in the M-SNELS imaging chamber and images were acquired by raster scanning the plate with the desired excitation and emission wavelength combinations.

## 2.9 Statistical Analysis

Variance analysis was performed to compare the effect of peptide treatment between control and treated animals using an *F* test. A paired *t* test was used to compare the effect of the peptide on the antigen-dependent response between F5 and CD2 T cells within the same animal. *P* values smaller than 0.05 were taken as significant. Statistical analysis was performed using Prism (GraphPad Software, Inc., La Jolla, CA).

## 3 Results

### 3.1 Efficiency in Experimental Detection of GFP and DsRed Expressing T Cells

First it was important to establish the technical capabilities and limitations of the M-SNELS methodology, which could then

be further optimized for the TCR-dependent antigen response experiment. Detection of CD2/GFP and F5/DsRed T cells in fact represented a challenge to the multicolor unmixing process since the targeted lymph nodes contained both cell populations and fluorescence was hence colocalized. Although the emission peaks for GFP ( $E_{m,max}$  520 nm) and DsRed ( $E_{m,max}$  590 nm) are separated by about 70 nm, their spectral profiles show a significant degree of overlap. Experimentally, the relative intensities of the two cell types will depend on fluorophore concentration (intra- and inter-cellular) and brightness, transcriptional activity of the reporter gene and on the anatomical location and size of the targeted cell population. Additionally, the total signal detected is dependent on the excitation and emission wavelengths used during image acquisition, which need to be taken into account for quantitative separation of multiple fluorescence intensities. In flow cytometry, spectral overlap is dealt with by applying a user-defined compensation factor during acquisition and has allowed detection of multiple fluorophores.<sup>33</sup>

In this study, GFP and DsRed emission cross-talk was significant (ranging between 10% to 20% of the total detected signal) and DsRed signal was weak, partly because GFP is brighter than DsRed, but also due to the excitation wavelengths available to the M-SNELS instrument (Figs. 1 and 2). GFP could in fact be excited very efficiently using a source at 488 nm (99% of maximum excitation) whereas the 514 nm source achieved approximately 50% of DsRed excitation. The sensitivity of the setup for DsRed detection could be further increased by the use of a yellow laser, currently not available in our lab. For the experiments reported here, the M-SNELS unmixing algorithm was optimized according to the relative intensities of CD2/GFP and F5/Dsred T-cells. For each cell type in fact, a calibration experiment allowed to calculate the spectral overlap in signal recorded by the setup (described below and in Sec. 2).

### 3.2 Validation of M-SNELS Quantification In Vitro and Spectral Strength Calculation

The quantification accuracy of the M-SNELS method was validated *in vitro* using increasing numbers of GFP and DsRed cells. Five concentrations of GFP and DsRed cells were fitted to a linear regression model ( $r^2 = 0.97$  and  $0.93$ , respectively) and demonstrated the sensitivity of M-SNELS in retrieving intensity values that correspond to an increase in concentration of fluorescent cells ranging from 0.2 to  $2 \times 10^5$  cells/ $\mu$ l [Fig. 3(a)]. The spectral strengths for both fluorophores at 540/40 nm and 615/90 nm were thus experimentally calculated using the mean fluorescence intensity value for each filter, across equal GFP and DsRed cell concentration ranges ( $n = 5$ ) (detailed in Sec. 2). At these wavelengths, nonspecific emissions (autofluorescence) are expected to be the major contributors to the reduced SNR. The experimentally determined spectral strength values allow selecting for the portion of signal regarded as positive fluorescence (in this case thresholded for GFP and DsRed) and dismissing all other signal as nonspecific, effectively reducing autofluorescence. Residual autofluorescence following unmixing is determined by the difference in excitation (of the nonspecific compounds) between the two wavelengths used. In this experimental setup, the difference between 488 and 514 nm, results in a negligible amount of residual autofluorescence that is significantly smaller than the error bars associated with M-SNELS data. However, complete removal of autofluorescence would require the measurement of

autofluorescence emission in a dedicated spectral window followed by a dedicated spectral unmixing step.

### 3.3 M-SNELS Imaging of T Cell Populations

The measured spectral strengths from the above *in vitro* experiment were used to calibrate the unmixing algorithm and applied *in vivo* where M-SNELS multicolor unmixing was tested for its ability to distinguish F5/DsRed- and CD2/GFP-expressing T-cells transferred in Rag1<sup>-/-</sup> immunodeficient mice. The cervical lymph nodes were chosen as the most suitable target due to the presence of closely located, symmetrical (left and right) nodes that have the added advantage of being easily imaged simultaneously. The left and right nodes were individually quantified and used as an internal control measure, since both LNs were expected to respond identically to peptide stimulation.

In order to validate the quantification accuracy of the unmixing algorithm, the M-SNELS intensities were compared to the results obtained by FACS (%) analysis for each LN ( $n = 8$ ) before (*mixed*) and after (*unmixed*) the unmixing step. The SNR (calculated as the ratio between the intensities in the ROI and the entire scanned area) for these samples ranged between 1:1 and 6:1. GFP and DsRed mean and standard deviation were calculated from averaging the left and right LNs, for both modalities, for each animal. While the *mixed* M-SNELS data showed poor correlation to FACS values ( $R^2 = 0.62$ ,  $p = 0.02$ ), the *unmixed* M-SNELS intensities showed a significant improvement in quantification accuracy ( $R^2 = 0.91$ ,  $p = 0.0002$ ) [Fig. 3(b) and 3(c)]. Therefore, following unmixing, GFP and DsRed emission intensities can be proportionally and quantitatively compared. M-SNELS quantification accuracy following spectral unmixing was further verified against absolute cell count determined by FACS and results matched the above performance by considerably improving quantification accuracy (*mixed*  $R^2 = 0.56$ , *unmixed*  $R^2 = 0.72$ ).

### 3.4 In Vivo Visualization of a TCR-Dependent Immune Response

The average time course for F5 T-cell proliferation in mounting of an anti-NP immune response in this experimental setup is estimated to be three to four days.<sup>27</sup> M-SNELS unmixing was used to follow *in vivo* the distinct responses of two T cell populations following cognate antigen administration (Fig. 4), where the F5/DsRed T cells recognize specifically the epitope carried by the injected peptide, whereas the CD2/GFP cells do not. M-SNELS unmixed data reveal that an initial F5/DsRed stability (one to two days after injection) is followed by a subsequent T cell clonal expansion, detectable three to four days after peptide stimulation [Fig. 4(b)]. Consistent with previous studies carried out on the same model,<sup>27</sup> an overall 277% increase in F5/DsRed intensity on day 4, respectively, to day 0 was recorded. Unexpectedly, the data also underline variability in kinetics between individual animals in terms of both magnitude and time frame of the response. In fact, depending on the animal, a decrease in F5/DsRed T-cell numbers was found to occur between days 1 and 2 whereas a peak F5/DsRed response was detected between day 3 and day 4 [Fig. 5(a)]. Since the response to NP administration is known not to diverge significantly between animals, this variability is likely indicative of experimental heterogeneity between animals. In fact, despite the fact that equal numbers of GFP and DsRed cells were injected in all mice, a noticeable difference in F5 lymphocytes

was detected on day 0 between animals (but not detected in GFP population).

The values recorded across the 5-day sampling period for the CD2/GFP cells showed a 15% decrease over time and was consistent with the variation detected in control nontreated animals used during the experimental optimization stages. Statistical analysis of values between day 0 and day 4 showed no significant difference in mean CD2/GFP population ( $p = 0.14$ ) but a significant difference in mean F5/DsRed population ( $p = 0.0092$ ) (paired *t* test) [Fig. 5(b)]. These data confirm that the DsRed population varies more than the GFP cells, in the same animals. However, since the CD8<sup>+</sup> F5/DsRed population was transferred together with polyclonal (CD2) cells, NP recognition by F5/DsRed was confirmed using control samples that had not been treated with NP.

Response to peptide administration was established by variance analysis (*F* test) between the control and NP-treated samples: only the NP-treated F5/DsRed population showed a statistically significant response compared to nontreated F5/DsRed ( $p = 0.0009$ ), nontreated CD2/GFP ( $p < 0.0001$ ) and NP-treated CD2/GFP ( $p < 0.0001$ ). Within the same time frame, the NP-treated CD2/GFP population showed no significant response compared to nontreated CD2/GFP ( $p = 0.24$ ) [Fig. 5(c)]. The CD2/GFP cells hence did not respond to the antigen stimulus, confirming that the F5/DsRed proliferation recorded was caused by NP recognition.

### 3.5 Assessment of Animal Individuality in Temporal Dynamics of T Cell Proliferation

It is well known that antigen-dependent T-cell activation gives rise to heterogeneous populations.<sup>34,35</sup> Certainly an associated, yet rarely addressed, question is what effect inter-animal variability has on the evaluation of antigen-dependent responses, even in artificial immune models such as the F5/NP. We compared the F5/DsRed time courses for each mouse and found significant variability in the dynamics of the response to identical treatment.

In order to evaluate whether this variability in response could be attributed to animal diversity or to experimental error, the coefficient of variation (CV, i.e., the ratio between the standard deviation and the mean) was calculated on the time course data and compared to control experiments [Fig. 5(d)]. Following peptide administration, the CV was 15.6% and 79.8% for CD2/GFP and F5/DsRed, respectively ( $n = 28$ ). In absence of peptide, the untreated LNs show a CV, over the same 5 day sampling period, of 8.3% and 45.8% for CD2/GFP and F5/DsRed, respectively ( $n = 8$ ). Whereas the CV between before (day 0) and after (day 4) peptide injection was 4.6% and 4.8% (CD2/GFP) and 8.4% and 20.9% for F5/DsRed LNs. These values were further evaluated against the CV associated to experimental error when repeatedly imaging (3x) equal GFP (3.3%) and DsRed (3.5%) samples *in vitro* ( $n = 10$ ). Cumulatively, the data indicate that CD2/GFP values are within experimental error variation and thus provide a solid control to the antigen-dependent response experiment, confirming that this population is not significantly affected by NP administration. The detected variation in F5/DsRed population was instead higher than that accounted for by experimental error or initial animal heterogeneity and can therefore be attributed to a population-specific individuality in temporal dynamics.

**Table 1** Spectral strengths for CD2/GFP and F5/DsRed.

gGFP	0.012525
gDsRed	-0.000410
rGFP	0.005725
rDsRed	0.0

Note: The spectral strengths used in the unmixing algorithm were obtained by solving Eq. (5) using the emission intensities recorded for known concentrations of CD2/GFP and F5/DsRed cells measured *in vitro*.

## 4 Discussion

M-SNELS was developed to overcome the limitations imposed on 3-dimensional imaging caused by low SNR levels, yet maintaining the advantages in signal quantification, provided by scanning the subject and normalizing the fluorescence with the excitation intensities. M-SNELS is a practical, robust and computationally nondemanding 2-dimensional imaging modality to which a spectral unmixing algorithm was successfully implemented, offering simultaneous feedback of two or more fluorescent reporters in low SNR conditions. Similar to its 3-dimensional counterpart, already sensitive to changes in fluorophore concentrations within pM and nM ranges,<sup>36,37</sup> M-SNELS signal intensity was shown here to depend in a linear manner on fluorophore concentration.

We examined its suitability in a biologically-relevant context where the kinetics of two T cell populations were monitored simultaneously. First, the M-SNELS setup was tested for its quantitative accuracy using cell culture plates where CD2/GFP and F5/DsRed cells were plated at concentrations ranging from 20,000 to 200,000 cells/ $\mu$ l: the linear dependency of fluorescence emission on cell concentration was thus validated. *In vitro* fluorescence intensities were used to accurately calibrate the unmixing algorithm according to the spectral overlap showed by these two fluorophores, specifically for the excitation and emission wavelengths available in the setup. M-SNELS unmixing was then validated *in vivo* and correlation between the mixed and unmixed fluorescence values with cell sorting showed a significant improvement to the goodness of fit following the unmixing step. The sensitivity range of the M-SNELS system, within the visible range, could be further improved by the use of a laser line closer to DsRed peak excitation, thereby increasing the SNR in the red channel.

An immunological response was induced in Rag1<sup>-/-</sup> mice, in which F5/DsRed and CD2/GFP-expressing T cells were concomitantly transferred. NP peptide injection induced a response only in the F5/DsRed cells expressing the specific TCR. The variation between CD2/GFP and F5/DsRed response to antigen recognition during an immunological response was then quantitatively described by M-SNELS imaging and the individual population time courses were scrutinized for specificity-dependent responses and animal heterogeneity.

M-SNELS *in vivo* data successfully distinguished between the responsive F5/DsRed population and the nonresponsive CD2/GFP cells and correctly reported the time course of the immune response, consistent with previously reported literature.<sup>27</sup> Our results showed that, in response to peptide, the F5/DsRed population increased on average 277% over five

days, whereas the CD2/GFP population, in the same animals, showed a 15% decrease. In the absence of the peptide, the F5/DsRed T-cells showed a 129% increase in the control sample over five days, whereas a 14% increase was recorded for the untreated CD2/GFP cells, consistent with a response to homeostatic cues. Adoptive transfer of T cells in lymphopenic hosts, in fact, results in an initial homeostatic expansion, followed by maintenance of stable T cell population numbers. Considering that the peptide response experiments described in this study were carried out 13 to 17 days after adoptive transfer, it was expected for the CD2/GFP cells to respond principally to homeostatic control mechanisms, aimed at maintaining stable overall number of T cells in peripheral lymphoid tissues. The F5/DsRed cells instead resulted in high proliferation rates, consistent with their capability of responding to both homeostatic cues and NP recognition. The good correlation ( $R^2 = 0.90$ ) between M-SNELS unmixed values and FACS data further support the validity of the *in vivo* results.

Currently, the measurement of changes in T-cell populations relies on testing large numbers of animals where inter-subject variability is often underestimated and assimilated to experimental error since results are discussed in terms of averages. It follows that a method suitable for testing the factors responsible for the variation of individual responses to antigen recognition and homeostasis, self-tolerance and immunosuppression would be of significant interest and could provide the means to manipulate the host immune response with improved specificity. As demonstrated here, the use of quantitative noninvasive optical techniques offers a simple alternative to current invasive methods and improves experimental data analysis, both qualitatively and quantitatively. *In vivo* detection of fluorescent signal in fact implies that the same animal can be followed over a series of time points, thus eliminating inter-animal variability during a longitudinal study. The limiting factor in an accurate description of a longitudinal time course therefore becomes the reproducibility of the individual time points, an issue that can be addressed during experimental design (e.g., by imaging the same animal in repeats) and that is associated with the instrumentation rather than with the biological activity of the sample. In this light, quantitative accuracy of *in vivo* fluorescence detection of superficial signals allows animal heterogeneity to be measured and treated as a parameter in its own right, rather than as a source of error.

## 5 Conclusions

M-SNELS was developed as an *in vivo* imaging approach that combines the ease of using epifluorescence methodologies with the quantitative accuracy provided by normalized fluorescence data, and is suitable for quantifying superficial low intensity fluorescence emissions in the visible spectrum. Coupled with multicolor detection using spectral unmixing, this method was successfully used to distinguish two T-cell populations with distinct dynamics, labeled with individual fluorophores. M-SNELS unmixing may be applied for monitoring patterns of cell proliferation, an essential aspect in immunological research for the characterization of T cell function and that could find applications in many other areas of research, such as preclinical oncology and metabolism, for the uncoupling of overlapping emission and absorption profiles and for the removal of autofluorescence. In conclusion, this study focuses on the wealth and novelty of data acquired using M-SNELS and demonstrates that, while it is possible to reproduce the data

obtained through standard invasive methodologies, an *in vivo* quantitative approach invariably provides accuracy to the results, consequently offering a more complete picture of the problem at hand.

### Acknowledgments

RF wishes to thank Dr. G. Fousteri for proofreading the manuscript. This work was supported by the FP7 EU Grant, FMT-XCT. R. Favicchio acknowledges a Marie Curie Early Stage Training grant (EST-MolecImag).

### References

1. A. D. Zacharopoulos et al., "A matrix-free algorithm for multiple wavelength fluorescence tomography," *Opt Express* **17**(5), 3025–3035 (2009).
2. A. Garofalakis et al., "Three-dimensional *in vivo* imaging of green fluorescent protein-expressing T cells in mice with noncontact fluorescence molecular tomography," *Mol. Imag.* **6**(2), 96–107 (2007).
3. G. Zacharakis et al., "Volumetric tomography of fluorescent proteins through small animals *in vivo*," *Proc. Natl. Acad. Sci. USA* **102**(51), 18252–18257 (2005).
4. G. Zacharakis et al., "Fluorescent protein tomography scanner for small animal imaging," *IEEE Trans. Med. Imag.* **24**(7), 878–885 (2005).
5. V. Ntziachristos and R. Weissleder, "Experimental three-dimensional fluorescence reconstruction of diffuse media by use of a normalized Born approximation," *Opt. Lett.* **26**(12), 893–895 (2001).
6. A. Soubret, J. Ripoll, and V. Ntziachristos, "Accuracy of fluorescence tomography in the presence of heterogeneities: study of the normalized Born ratio," *IEEE Trans. Med. Imag.* **24**(10), 1377–1386 (2005).
7. G. Zacharakis et al., "Spectroscopic detection improves multi-color quantification in fluorescence tomography," *Biomed. Opt. Express* **2**(3), 431–439 (2011).
8. M. Simantiraki et al., "Multispectral unmixing of fluorescence molecular tomography data," *JIOHS* **2**(4), 353–364 (2009).
9. T. Zimmermann, "Spectral imaging and linear unmixing in light microscopy," *Adv. Biochem. Eng. Biotechnol.* **95**, 245–265 (2005).
10. G. Themelis, J. S. Yoo, and V. Ntziachristos, "Multispectral imaging using multiple-bandpass filters," *Opt. Lett.* **33**(9), 1023–1025 (2008).
11. M. Ducros et al., "Spectral unmixing analysis of performance in the olfactory bulb *in vivo*," *PLoS ONE* **4**(2), e4418 (2009).
12. G. Zacharakis et al., "Normalized transillumination of fluorescent proteins in small animals," *Mol. Imag.* **5**(3), 153–159 (2006).
13. V. Ntziachristos et al., "Planar fluorescence imaging using normalized data," *J. Biomed. Opt.* **10**(6), 064007 (2005).
14. J. M. Tam et al., "Improved *in vivo* whole-animal detection limits of green fluorescent protein-expressing tumor lines by spectral fluorescence imaging," *Mol. Imag.* **6**(4), 269–276 (2007).
15. C. C. Pritchard et al., "Project normal: defining normal variance in mouse gene expression," *Proc. Natl. Acad. Sci. USA* **98**(23), 13266–13271 (2001).
16. A. W. Goldrath et al., "The molecular program induced in T cells undergoing homeostatic proliferation," *Proc. Natl. Acad. Sci. USA* **101**(48), 16885–16890 (2004).
17. J. H. Chewing et al., "Bioluminescence-based visualization of CD4 T cell dynamics using a T lineage-specific luciferase transgenic model," *BMC Immunol.* **10**, 44 (2009).
18. M. Azadniv et al., "CD4+ T cell effects on CD8+ T cell location defined using bioluminescence," *PLoS ONE* **6**(1), e16222 (2011).
19. M. R. Patel et al., "Longitudinal, noninvasive imaging of T-cell effector function and proliferation in living subjects," *Cancer Res.* **70**(24), 10141–10149 (2010).
20. M. J. Pittet, "In vivo imaging of T cell delivery to tumors after adoptive transfer therapy," *Proc. Natl. Acad. Sci. USA* **104**(30), 12457–12461 (2007).
21. R. C. Koya et al., "Kinetic phases of distribution and tumor targeting by T cell receptor engineered lymphocytes inducing robust antitumor responses," *Proc. Natl. Acad. Sci. USA* **107**(32), 14286–14291 (2010).
22. A. Sarantopoulos, G. Themelis, and V. Ntziachristos, "Imaging the bio-distribution of fluorescent probes using multispectral epi-illumination cryoslicing imaging," *Mol. Imag. Biol.* **13**(5), 874–885 (2011).
23. S. Celli et al., "Decoding the dynamics of T cell-dendritic cell interactions *in vivo*," *Immunol. Rev.* **221**, 182–187 (2008).
24. T. R. Mempel et al., "T-cell priming by dendritic cells in lymph nodes occurs in three distinct phases," *Nature* **427**(6970), 154–159 (2004).
25. H. Veiga-Fernandes et al., "Tyrosine kinase receptor RET is a key regulator of Peyer's Patch organogenesis," *Nature* **446**(7135), 547–551 (2007).
26. C. Mamalaki et al., "Positive and negative selection in transgenic mice expressing a T-cell receptor specific for influenza nucleoprotein and endogenous superantigen," *Dev. Immunol.* **3**(3), 159–174 (1993).
27. C. Mamalaki et al., "Thymic depletion and peripheral activation of class I major histocompatibility complex-restricted T cells by soluble peptide in T-cell receptor transgenic mice," *Proc. Natl. Acad. Sci. USA* **89**(23), 11342–11346 (1992).
28. C. Mamalaki et al., "T cell deletion follows chronic antigen specific T cell activation *in vivo*," *Int. Immunol.* **5**(10), 1285–1292 (1993).
29. J. de Boer et al., "Transgenic mice with hematopoietic and lymphoid specific expression of Cre," *Eur. J. Immunol.* **33**(2), 314–325 (2003).
30. E. Spanopoulou et al., "Functional immunoglobulin transgenes guide ordered B-cell differentiation in Rag-1-deficient mice," *Genes Dev.* **8**(9), 1030–1042 (1994).
31. E. Spanopoulou, "Cellular and molecular analysis of lymphoid development using Rag-deficient mice," *Int. Rev. Immunol.* **13**(4), 257–288 (1996).
32. E. Spanopoulou et al., "The homeodomain region of Rag-1 reveals the parallel mechanisms of bacterial and V(D)J recombination," *Cell* **87**(2), 263–276 (1996).
33. T. S. Hawley et al., "Four-color flow cytometric detection of retrovirally expressed red, yellow, green, and cyan fluorescent proteins," *Biotechniques* **30**(5), 1028–1034 (2001).
34. S. M. Kaech and E. J. Wherry, "Heterogeneity and cell-fate decisions in effector and memory CD8+ T cell differentiation during viral infection," *Immunity* **27**(3), 393–405 (2007).
35. D. L. Woodland and R. W. Dutton, "Heterogeneity of CD4(+) and CD8(+) T cells," *Curr. Opin. Immunol.* **15**(3), 336–342 (2003).
36. M. Nahrendorf et al., "Hybrid PET-optical imaging using targeted probes," *Proc. Natl. Acad. Sci. USA* **107**(17), 7910–7915 (2010).
37. A. Garofalakis et al., "In vivo validation of free-space fluorescence tomography using nuclear imaging," *Opt. Lett.* **35**(18), 3024–3026 (2010).